

DISTRIBUTED HIGH FREQUENCY EFFECTS IN BIPOLAR TRANSISTORS

M.P.J.G. Versleijen

Philips Research Laboratories, 5600 JA Eindhoven, The Netherlands

Abstract

The relevance of distributed high frequency effects in modern bipolar transistors is investigated. Simple approximations for compact modelling are given and their performance is shown by comparison with device simulations and measurements.

Introduction

Compact bipolar transistor models for circuit simulation are usually defined as lumped circuit models. Because of the distributed nature of the transistor this approach becomes invalid at high signal frequencies. It is possible to distinguish between vertical Non-Quasi-Static (NQS) effects (along the collector current trajectories) and lateral ac crowding effects. The first have a one-dimensional (1D) nature whereas the latter are essentially 2D. Both are successively treated below. Distributed effects become noticeable when signal frequencies approach and exceed certain characteristic frequencies. For vertical NQS effects this is the maximum common-emitter cut-off frequency, f_T . For ac crowding the reciprocal intrinsic RC time, denoted here with f_{ac} , is indicative. Beyond these frequencies the transistor performance degrades and useful application within circuits becomes difficult. An accurate description of device behaviour up to f_T or f_{ac} therefore is sufficient for most circuit simulation applications. To fulfil this condition, simple, minimum component, lumped circuit approximations, usable for compact modelling, will be given and are tested against ac device simulations. Their performance is also demonstrated by comparison with measurements.

Vertical NQS effects

Vertical NQS effects result from the finite carrier diffusivity and velocity. They become noticeable as delay (or excess phase shift) at frequencies approaching the reciprocal carrier transit times, which is around the maximum f_T . An exact description of NQS transistor behaviour requires the solution of the time dependent charge transport equations. General solutions of these equations for separate regions can be obtained but, because of their transcendental nature are not suitable for compact modelling. In practice low frequency approximations of the exact solution can be used. The simplest is known as the Charge Control Concept [1] which only describes quasi-static device behaviour; i.e. the collector current and stored base charge instantaneously follow the applied base voltage. In addition several approaches have been proposed to account for NQS device behaviour. Mostly only delay effects in the neutral base are consid-

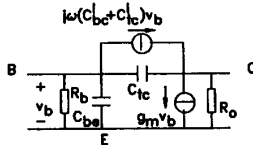


Figure 1: Hybrid- π , small-signal equivalent circuit for 1D transistor structure.

ered [2,3,4]. Sometimes also NQS neutral emitter effects, affecting the input admittance but not the transadmittance, are treated [5,6]. Some approaches (e.g. those employing time delay elements) can not easily be implemented into large-signal models, while others are less attractive because they need extra internal voltage nodes. Furthermore, in a modern transistor the transit time is distributed over the total device. Especially the delay in the base-collector depletion region is not negligible. For a practically useful compact model all regions should be modelled with comparable accuracy.

In this paper a minimum component, hybrid- π circuit model (see fig. 1) without internal nodes is considered to describe 1D ac device behaviour. The circuit follows from a 1D large-signal model. The use of a physical charge-description leads to the controlled capacitance between base and collector, which is absent in conventional hybrid- π transistor models. This transcapacitance accounts for both neutral base and base-collector depletion region delay.

Using stored base-charge partitioning [4], the first term of this element ($j\omega C_{bc}^I$; see fig. 1) models the delay encountered by the collector current passing the neutral base. The involved transcapacitance is defined as

$$C_{bc}^I = p_c \left. \frac{\partial Q_{be}}{\partial V_{be}} \right|_{V_{bc}}, \quad (1)$$

with Q_{be} the forward-bias base diffusion charge and p_c the fraction of Q_{be} that is reclaimable via the base-collector junction. p_c depends on the base doping profile and injection level. For a homogeneously doped base and low level injection $p_c = 0.33$, whereas at high injection $p_c = 0.5$.

The second term of the transcapacitance ($j\omega C_{ic}^I$) originates from the current dependence of the base-collector depletion charge [7,8,9] and is for a homogeneously doped epilayer given by

$$\begin{aligned} C_{ic}^I &= \left. \frac{\partial Q_{ic}}{\partial V_{be}} \right|_{V_{bc}} \\ &= g_m r_{cv} \left(1 - \frac{d}{W_{epi}}\right) C_{ic} + g_m \frac{d}{2v_s}, \end{aligned} \quad (2)$$

with $g_m = \left. \frac{\partial I_c}{\partial V_{be}} \right|_{V_{bc}}$ the transconductance, $C_{ic} = \left. \frac{\partial Q_{ic}}{\partial V_{bc}} \right|_{I_c}$ the normal base-collector depletion capacitance, r_{cv} the vertical collector epilayer resistance, d the base-collector depletion width, W_{epi} the epilayer width and v_s the saturated drift velocity of electrons. The first term in (2) accounts for the internal Miller effect as caused by the resistance of the undepleted part of the epilayer. The second term accounts for the delay of the collector current passing the depletion layer.

element definition	value
$R_b = Re(y_{11})^{-1}$	58.1k Ω
$R_0 = Re(y_{22})^{-1}$	747k Ω
$g_m = Re(y_{21})$	1.30mS
$C_{bc} = \frac{1}{\omega}(Im(y_{11}) + Im(y_{21}))$	16.07fF
$C_{ic} = -\frac{1}{\omega}Im(y_{12})$	0.21fF
$C_{bc}^I + C_{ic}^I = -\frac{1}{\omega}(Im(y_{21}) - Im(y_{12}))$	11.88fF

Table I: Element values for the hybrid- π circuits of figs. 1 and 4. Values are given for a $1\mu\text{m}^2$ emitter area and at a bias setting of $V_{BE} = 0.8\text{V}$ and $V_{BC} = -1.0\text{V}$, which is around the maximum f_T .

The performance of the hybrid- π circuit of fig. 1 is compared with 1D ac device simulations. For the sake of convenience a piecewise constant doping profile (emitter: 10^{20}cm^{-3} $0.2 \mu\text{m}$, base: $2 \cdot 10^{17} \text{cm}^{-3}$ $0.2 \mu\text{m}$, collector epilayer: 10^{16}cm^{-3} $1.0 \mu\text{m}$, collector buried layer: $5 \cdot 10^{19} \text{cm}^{-3}$ $0.6 \mu\text{m}$) is used. More realistic profiles, however, give similar results. The hybrid- π element values are obtained from low frequency common-emitter y -parameters as given in table I.

From fig. 2 it is seen that the phase of $y_{21} (= \frac{i_c}{v_{be}} \Big|_{v_{ce}=0})$ (or delay of the collector current) is accurately described by the lumped circuit up to f_T , while the error in the amplitude remains small. The importance of a physical charge-description is illustrated by the fact that the delay is completely due to the controlled capacitance. From a regional transit time analysis [8] the controlled capacitance can be resolved in its separate terms. It is found that $C_{ic}^I = 4.3 \text{fF}$. So a significant part (36%) of the collector current delay is caused by the current dependent base-collector depletion charge. This is typical for analog devices having a relatively lightly doped and thick epilayer. Because no internal nodes are present in the hybrid- π circuit, the charge instantaneously follows the applied voltage. Thus at high frequencies the lumped circuit $y_{11} (= \frac{i_b}{v_{be}} \Big|_{v_{ce}=0})$ becomes fully capacitive. This is not in agreement with the device simulation results which tend to deviate from ideal capacitive behaviour around f_T . This is due to the delayed built-up of base as well as emitter diffusion charge. Approximate modelling with a lumped circuit is only possible by the introduction of internal nodes. However, especially the delay of the emitter charge is difficult to quantise [10]. Furthermore, it will be shown later, that ac current crowding and/or extrinsic parasitics generally overrule delay effects on the intrinsic y_{11} . More accurate modelling therefore is not considered here. It can be concluded that a hybrid- π equivalent circuit model, based on a physical large-signal model, accurately describes the phase of y_{21} up to f_T .

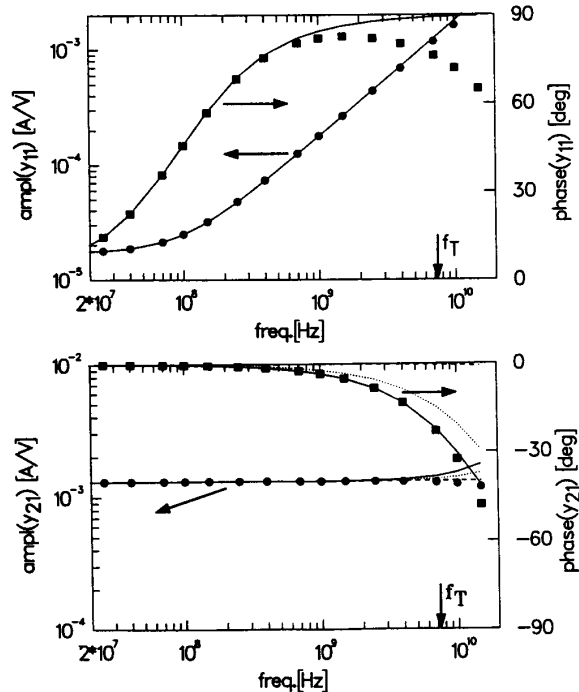


Figure 2: Common-emitter input admittance, y_{11} and transadmittance, y_{21} versus frequency. Comparison of 1D ac device simulations (\bullet \blacksquare), hybrid- π model (—), hybrid- π : $C_{ic}^I = 0$, (\cdots) and conventional hybrid- π : $C_{bc}^I + C_{ic}^I = 0$ (---). The hybrid- π element values are given in table I.

ac current crowding

Ac current crowding is a consequence of the distributed RC nature in the lateral direction along the intrinsic base. At high frequencies this results in non-uniform vertical ac currents, thus affecting the small-signal base and collector currents [11,12]. The input impedance seen at the base terminal can be considered as an open RC transmission line. When there is no significant DC crowding ($R_B I_b < V_T$, with V_T the thermal voltage), the transmission line is uniform and the exact input impedance is given by [11]

$$Z_b = \sqrt{\frac{R_B}{Y_b}} \coth \sqrt{Y_b R_B}, \quad (3)$$

where R_B is the lateral internal base series resistance and $Y_b (= R_b^{-1} + j\omega C_b)$ (see fig. 1) is the total vertical admittance from base to emitter and collector. R_b is the differential base-emitter resistance. C_b includes the base-emitter and base-collector depletion as well as the emitter and base diffusion capacitances. Equation (3) is valid for a transistor with a single base contact. The double base contacted situation is also described by (3) when R_B is replaced by $R_B/4$.

The main characteristic of a distributed RC input impedance is its asymptotic 3dB/oct amplitude fall off, which can not be modelled by a finite number of conventional network elements. Of practical relevance is behaviour at frequencies not too far beyond the first zero of Z_b . An equivalent circuit approximation having one internal node is found from series expansion in $j\omega$ of (3) and leads to

$$Z_b^{(2)} = \frac{1}{R_{BV}^{-1} + j\omega C_{ac}} + \frac{1}{R_b^{-1} + j\omega C_b}. \quad (4)$$

Here an effective base series impedance (first term) is put in series with the total internal vertical impedance. The series impedance comprises the well known effective base series resistance, $R_{BV} (= \frac{R_B}{3})$ shunted by an ac crowding capacitance, $C_{ac} (= \frac{C_b}{5})$. In fig. 3 it is shown that C_{ac} increases the valid frequency range of Z_b with a factor of 4. By making R_{BV} and C_{ac} bias dependent, (4) can also be used when (weak) DC crowding occurs, hereby making the effective series impedance formulation suitable for a large-signal compact model.

A simple criterion to estimate the importance of ac crowding in comparison with vertical NQS effects follows from the involved time constants: $\tau_{ac} = (2\pi f_{ac})^{-1} = \frac{R_B C_b}{3}$ and $\tau_T = (2\pi f_T)^{-1} = \frac{C_b}{g_m} = \frac{C_b V_T}{I_c}$. When $\tau_{ac} > \tau_T$, or equivalently, $R_B I_c > 3V_T$, ac crowding becomes

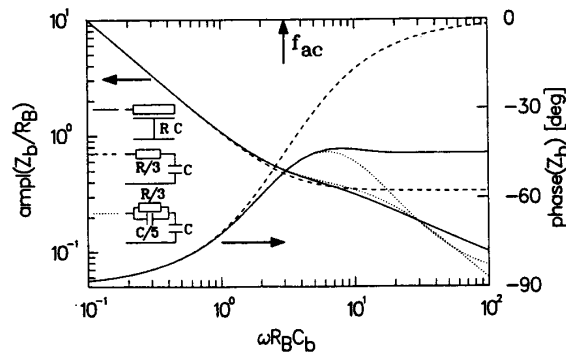


Figure 3: RC transmission line input impedance versus frequency. Exact solution (—), approximation with C_{ac} (\cdots) and without C_{ac} (---).

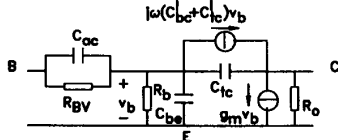


Figure 4: Small-signal equivalent circuit for 2D transistor structure.

relevant at lower frequencies than vertical NQS effects. At a given collector current density this occurs when the emitter width (H_e) exceeds a critical value given by

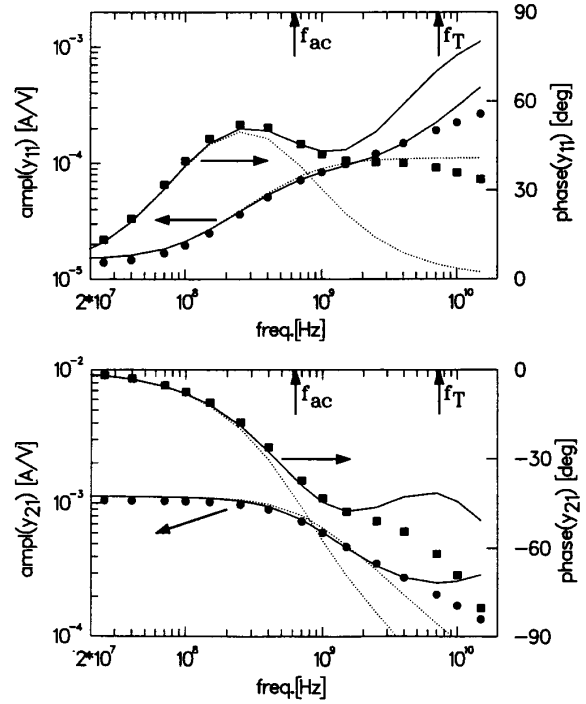
$$H_e^{crit} = \sqrt{\frac{3V_T}{\rho_B J_c}}, \quad (5)$$

with ρ_B the bias dependent base sheet resistance and J_c the collector current density. For a transistor with two base contacts H_e^{crit} is doubled. Note also that ac crowding may be relevant before DC crowding occurs ($R_B I_B > V_T$). The above considerations clearly show the importance of an accurate effective base series impedance model. To model ac crowding the equivalent circuit of fig. 1 is extended as shown in fig. 4. The performance of this circuit is estimated by comparison with a 2D ac device simulation (see fig. 5). The same vertical doping profile, emitter area and bias setting as for fig. 2 is used. The emitter width now is $2\mu\text{m}$ and the base is contacted at one side only. The impact of lateral resistance effects on forward y-parameters is seen by comparing figs. 2 and 5. The distributed resistance effects are clearly demonstrated by the asymptotic amplitude slopes of y_{11} and y_{21} . In the case of a constant base series resistance y_{11} reaches a constant value whereas y_{21} shows 6dB/oct fall off. This is modelled by the equivalent circuit without C_{ac} . In the distributed case y_{21} falls off less while y_{11} keeps rising. This behaviour is approximated by addition of C_{ac} and increases the valid frequency range from f_{ac} to $4f_{ac}$. At the given bias setting DC crowding is still unimportant ($R_B I_B \approx 10\text{mV} < V_T$). The emitter width however, is too large to obtain model agreement up to f_T ($H_e = 2\mu\text{m}$ whereas $H_e^{crit} \approx 0.5\mu\text{m}$). Assuming that the local current gain is independent of the lateral position, it can be shown that y_{11} and y_{21} are influenced in the same way by ac crowding. Consequently the current gain $h_{21}(= \frac{y_{21}}{y_{11}})$, and thus f_T , are not affected.

Comparison with measurements

In an actual transistor several parasitics may influence the terminal small-signal behaviour and therefore must be included in a lumped circuit model. The circuit of fig. 6 represents the relevant parts of the MEXTRAM model. MEXTRAM [13] is an advanced large-signal bipolar transistor model provided, among other things, with a physically based charge-description. Explicitly modelled are the extrinsic emitter, base and collector series resistances (R_E , R_{BC} and R_{CC} in fig. 6). The extrinsic base-collector depletion capacitance is split up in two parts (C_{tcxx} and C_{tcx}). The extrinsic RC time generally is much smaller than the intrinsic one. Therefore distributed effects in the extrinsic transistor are negligible. Also the base-emitter sidewall capacitance (C_{tcx}) and substrate parasitics (C_{SUB} and R_{SUB}) are explicitly accounted for. Generally the importance of parasitics can be estimated by examination of the associated time constants.

In fig. 7 small-signal measurements of a transistor from an advanced self-aligned process [14], with emitter dimensions on silicon of $2.5 \times 18.5\mu\text{m}^2$ and with a double base contact are compared with the MEXTRAM calculations. The measurements are performed on wafer and corrected for layout parasitics as described in [15]. Also model calculations without the ac crowding capacitance and without the controlled capacitance are given. For the specific emitter width ac crowding effects clearly overrule vertical NQS effects. It can be


 Figure 5: Common-emitter input admittance, y_{11} and transadmittance, y_{21} versus frequency for 2D transistor structure. Comparison of 2D ac device simulations (\bullet , \blacksquare), hybrid- π circuit with C_{ac} (—) and hybrid- π circuit without C_{ac} (\cdots). $R_{BV} = 9\text{k}\Omega$ and $C_{ac} = 5.6\text{fF}$, other element values as given in table I.

concluded that the high frequency compact model performance is significantly improved when a simple ac crowding model and a physical charge-description is used. As expected, the current gain is almost insensitive for the ac crowding model. In addition also measurements and model calculations of a $0.5 \times 18.5\mu\text{m}^2$ emitter device are shown in fig. 8. Here transadmittance fall off is dominated by the extrinsic base resistance and ac crowding is hardly relevant. Again excellent model agreement up to f_T is obtained. It is instructive to compare the high frequency behaviour of both devices. For $f > 3\text{GHz}$ y_{11} and y_{21} are almost equal. So at high frequencies the wide emitter device, in spite of its larger DC current, performs similar as the narrow emitter device.

Similar agreement between model and measurements is obtained for other devices, other small-signal parameters and at other bias settings.

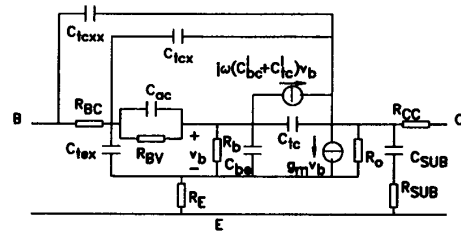


Figure 6: Relevant parts of the small-signal equivalent circuit of the MEXTRAM model.

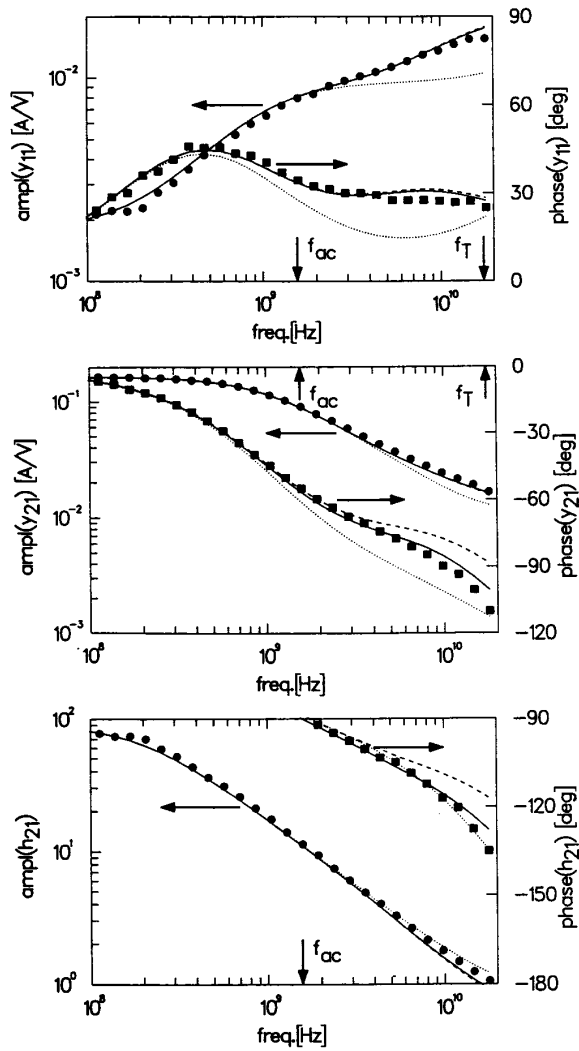


Figure 7: Common-emitter input admittance, y_{11} , transadmittance, y_{21} and current gain, h_{21} versus frequency. Comparison of measurements of a $2.5 \times 18.5 \mu\text{m}^2$ emitter device ($\bullet \blacksquare$), complete MEXTRAM model (—), MEXTRAM without C_{ac} (\cdots) and MEXTRAM without controlled capacitance ($---$). The transistor is biased at $V_{BE} = 0.85\text{V}$ and $V_{BC} = 0\text{V}$, which is around the maximum f_T .

Conclusions

The origin of distributed high frequency effects in bipolar transistors was reviewed. The occurrence of these distributed effects as a function of frequency was related to the approach of characteristic frequencies; f_T and f_{ac} for vertical and lateral effects respectively. It was shown that a hybrid- π ac model provided with a transcapacitance between base and collector correctly predicts the phase of the transadmittance up to f_T . The transcapacitance value naturally follows from a physical large-signal charge model and incorporates neutral base as well as base-collector depletion region delay. Ac crowding in the internal base can be effectively modelled by adding a capacitor in parallel to the intrinsic base resistance. The capacitance value is related to the total input capacitance at the base. It was also shown that ac crowding may be relevant at bias settings before DC crowding occurs and significantly influences the forward y -parameters. Ac crowding however, has no influence on the current gain. Furthermore, a critical emitter width was defined making

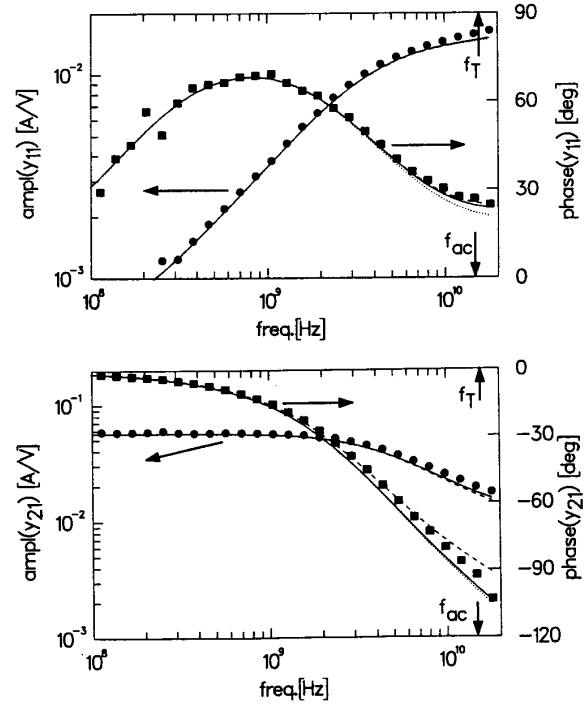


Figure 8: Common-emitter input admittance, y_{11} and transadmittance, y_{21} versus frequency. Comparison of measurements of a $0.5 \times 18.5 \mu\text{m}^2$ emitter device ($\bullet \blacksquare$), complete MEXTRAM model (—), MEXTRAM without C_{ac} (\cdots) and MEXTRAM without controlled capacitance ($---$). The transistor is biased at $V_{BE} = 0.85\text{V}$ and $V_{BC} = 0\text{V}$, which is around the maximum f_T .

it possible to determine when ac crowding dominates vertical NQS effects. Finally it was shown that when the model for the intrinsic transistor is properly extended with parasitic elements, as has been done in the MEXTRAM model, hf small-signal transistor behaviour can be correctly simulated up to the highest frequencies of practical interest.

Acknowledgement

The author wishes to express his appreciation to J.A.M. Geelen for performing the hf measurements and to R. Dekker for software contributions.

References

- [1] R. Beaufoy et. al., A.T.E.J. 13, 310 (1957).
- [2] J. te Winkel, IEEE Trans. Electr. Dev. ED-20, 389 (1973).
- [3] J.A. Seitchik et. al., IEEE IEDM 1987, paper 11.1.
- [4] H. Klose et. al., IEEE Trans. Electr. Dev. ED-34, 1090 (1987).
- [5] B.S. Wu et. al., IEEE Trans. Electr. Dev. ED-36, 727 (1989).
- [6] G.A.M. Hurkx, Solid State Electr. Vol-31, 1269, (1988).
- [7] F.N. Trofimenkoff, Proc. IEEE, 86 (1964).
- [8] J.J.H. van den Biesen, Solid State Electr. Vol-29, 529 (1986).
- [9] R.G. Meyer et. al., IEEE Trans. Electr. Dev. ED-34, 450, (1987).
- [10] J.A. Seitchik, IEEE Trans. Electr. Dev. ED-37, 2108, (1990).
- [11] R.L. Pritchard, Proc. IRE, 1152 (1958).
- [12] H.N. Gosh, IEEE Trans. Electr. Dev. ED-12, 513 (1965).
- [13] H.C. de Graaff et. al., IEEE BCTM 1989, paper 9.3.
- [14] J. van der Velden et. al. IEEE IEDM 1989, paper 9.4.
- [15] M.C.A.M. Koolen et. al., IEEE BCTM 1991.